Short- and medium range order in GeTe4-Ag glasses

P. Jóvári, V Nazabal, C. Boussard, S. Cui, I Kaban, S. Michalik, M. A. Webb, D. Le Coq, R. Chernikov, N. Chen, et al.

Short- and medium range order in $GeTe_4$-Ag glasses

P Jóvári[a], V Nazabal[b], C Boussard[b], S Cui[b], I Kaban[c], S Michalik[d], M A Webb[e], D Le Coq[b], R Chernikov[e], N Chen[e], J Darpentigny[f]

[a]Wigner Research Centre for Physics, Institute for Solid State Physics, H-1525 Budapest, POB 49, Hungary

[b]Institut Sciences Chimiques de Rennes, UMR-CNRS 6226, Campus de Beaulieu, Université de Rennes 1, 35042 Rennes Cedex, France

[c]IFW Dresden, Institute for Complex Materials, Helmholtzstr. 20, 01069 Dresden, Germany

[d]Diamond Light Source Harwell Science and Innovation Campus, Didcot, Oxfordshire, OX11 0DE, UK

[e]Canadian Light Source, 44 Innovation Blvd, Saskatoon, SK, Canada

[f]Laboratoire Léon Brillouin, CEA-Saclay 91191 Gif sur Yvette Cedex France

Abstract

Short- and medium range order glasses of $GeTe_4$-Ag approximate composition have been studied by neutron diffraction, X-ray diffraction and extended X-ray absorption fine structure spectroscopy. Chemical correlations have been determined by fitting multiple datasets simultaneously with the reverse Monte Carlo simulation technique. It has been found that Ge atoms remain basically fourfold coordinated by Te while Te atoms have mostly two Ge/Te neighbours. The topology of the $GeTe_4$ host network does not change upon adding Ag. Similarly to binary Ge-Te glasses, neighbouring $GeTe_4$ tetrahedra are predominantly in corner sharing configuration in all investigated $GeTe_4$-Ag compositions. Ag atoms bind mostly to Te and the average total coordination number of Ag does not change significantly with increasing Ag content.

Introduction

Ge-Te based glasses are widely applied in infrared optics due to their high transmission in the 2-20 μm range [1]. The production of various optical elements (e.g. fibers and lenses) requires a broad supercooled liquid region where these alloys can be shaped without the onset of crystallization. Binary Ge-Te alloys can be vitrified only by very fast cooling [2] but their poor glass forming ability can be improved by adding Ga, Se, I, Ag or AgI [3-4].

Short range order in Ge-Te and different Ge-Te-based glasses has been investigated by the reverse Monte Carlo simulation technique (RMC) using neutron diffraction, X-ray diffraction and various EXAFS datasets to produce models compatible with experimental data. In binary Ge_xTe_{100-x} glasses

($14 \leq x \leq 24$) coordination numbers of Ge and Te obtained by unconstrained simulation are very close to 4 and 2, respectively [5]. It is to be emphasized that apart from some basic input parameters (density, minimum interatomic distances) no prior structural information was used in these calculations. Thus it follows directly from the experimental data that both Ge and Te satisfy the 8-N rule. Additives (Ga, Ag or AgI, Se, I) affect the structure of the host Ge-Te network in different ways. According to a combined RMC-density functional theory study of $Ga_{11}Ge_{11}Te_{78}$ [6] Ga atoms are mostly fourfold coordinated and increase the average coordination number of Te. A more recent experimental study has shown that corner- and edge sharing $GeTe_4$ and $GaTe_4$ tetrahedra form a network in $Ge_xGa_xTe_{100-2x}$ ($7.5 \leq x \leq 14.3$) glasses [7]. Both RMC and first principles molecular dynamics simulations revealed that I binds mainly to Ge and decreases the average connectivity of the glass network in $Ge_{20}Te_{73}I_7$ [8, 9]. Se also binds preferentially to Ge in $Ge_{20}Se_{10}Te_{70}$ and the Se/Te substitution does not change the average coordination number of this network [10]. Ge atoms are tetrahedrally coordinated in all of the above mentioned glasses.

The most drastic structural rearrangement is induced by introduction of AgI. In these glasses, I binds mostly to Ge thus the number of Ge-Te bonds decreases. One would expect then the increase of Te-Te coordination and the formation of Te chains. Detailed structural investigations revealed that the Ge-Te network structure adopts to AgI in a different way. In $0.75GeTe_4$-0.25AgI, the total coordination number of Te, N_{Te}, is close to 3. It is to be emphasized that not only N_{Te} increases but the average number of Ge and Te atoms around Te is also higher than 2 (2.76 ± 0.3 [11]). Thus, upon adding AgI a significant percentage of Te atoms switches to threefold coordination (meaning also that formation of longer –Te-Te-Te- chains is unlikely). Ag binds mostly to Te but Ag-I bonding was also detected. The stability of $GeTe_4$-AgI glasses and supercooled liquids also exhibits a remarkable composition dependence: the glass transition temperature (T_g) decreases while the width of the supercooled liquid region increases with increasing AgI content. This behaviour suggests that addition of AgI destabilizes the $GeTe_4$ covalent network but it also hinders the onset of crystallization in the supercooled liquid state.

We are not aware of simulation studies (either experimental or first principle molecular dynamics) discussing the structure of Ge-Te-Ag glasses. In the present work, we investigate the short- and medium range order of $GeTe_4$-Ag glasses. Large scale structural models are obtained by the reverse Monte Carlo simulation technique [12], a platform for fitting diffraction and EXAFS data [13] simultaneously. Models will be compared with those of binary Ge-Te glasses [5], $Ge_{20}Te_{73}I_7$ [8] and $0.75GeTe_4$-0.25AgI [11]. Changes in the environment of Ge and Te atoms and the connectivity of Ge-centred structural units in the above Ge-Te based glasses will be discussed in detail.

Experimental

$GeTe_4$-Ag glasses were prepared from Te (5N), Ge (5N), and Ag (5N). Raw materials were introduced in a silica tube sealed under vacuum and placed in a rocking furnace. Glasses were obtained by melting and homogenization of chemical reagents at 750 °C for 10 h, and then the liquid was quenched from 500 °C. The glassy samples were annealed at 5 °C below the respective glass-transition temperature T_g for 3 h. Sample compositions were determined by energy dispersive X-ray spectroscopy (see Table 1).

The neutron diffraction measurement was carried out at the 7C2 diffractometer [14] of Laboratoire Léon Brillouin (France). Powdered samples were filled into vanadium sample holders of 6 mm diameter and 0.1 mm wall thickness. Scattered intensities were recorded with a multidetector system of 256 position sensitive tubes filled with ^{3}He. Detector efficiency was measured by means of vanadium powder while detector position and wavelength of incident neutrons (0.723 Å) were determined by a standard Ni powder sample. Raw data were corrected for background scattering, detector efficiency and absorption. We note that the neutron absorption cross section of Ag is significant [15]. Nevertheless, due to the moderate Ag content and the loose space filling of powder samples standard correction procedures (e.g. that of Paalman and Pings [16] implemented for neutron diffraction) can handle it.

High energy X-ray diffraction measurements were performed at the Joint Engineering, Environmental and Processing (I12-JEEP) beamline at Diamond Light Source Ltd (UK). The wavelength and size of the incident X-ray beam was 0.1439 Å and 200 × 200 μm^2. The sample material was loaded into a borosilicate capillary with the diameter of 1 mm. Diffraction data were collected in transmission geometry by a flat type detector Pilatus 2M CdTe with the active area of 253.7 × 288.8 mm^2 and the pixel size of 172 × 172 μm^2. The sample-to-detector distance was 322 mm. Diffraction data were integrated into reciprocal space using the DAWN software [17]. Raw intensities were corrected for background scattering (empty capillary and air contribution), sample absorption, fluorescence and Compton scattering to obtain the elastically scattered intensity using the PDFGetX2 software [18]. Elastically scattered X-ray intensities were used to calculate the total X-ray structure factors applying the Faber-Ziman formalism [19].

EXAFS measurements were performed in transmission mode at the Canadian Light Source (CLS). For this, the glasses were finely ground, mixed with cellulose, and pressed into tablets. Ag and Te EXAFS spectra were measured at beamline CLS 06ID-1 Hard X-ray Micro-Analysis (HXMA). Radiation from a superconducting wiggler source was monochromatised by a Si(220) crystal pair. To reject higher harmonics the double crystal monochromator was detuned to about 20% and 30% for Ag and Te EXAFS scans, respectively. Ge K-edge spectra were obtained at the CLS 07ID-2M Biological X-ray Absorption Spectroscopy (BioXAS) main beamline. The X-rays from a wiggler were monochromatized by a Si(220) double-crystal which was detuned to 50% of the maximum intensity to suppress higher harmonics. The energy was calibrated using an Ag foil for the Ag K-edge, GeO_2 for the Ge K-edge and Sb foil for the Te K-edge.

EXAFS data were corrected using the Viper programme [20]. Raw $k^3\chi(k)$ data were Fourier transformed to real space and then back transformed using rectangular windows (Ge: 1.65 Å -2.8 Å, Ag: 1.50 Å – 3.0 Å, Te: 1.50 Å - 3.2 Å). The filtered $k^3\chi(k)$ curves were used in reverse Monte Carlo simulations.

Reverse Monte Carlo simulation

The reverse Monte Carlo technique is a simulation method that produces structural models by fitting experimental data (mostly diffraction and EXAFS) along with various constraints (e. g. minimum interatomic distances, coordination constraints, bond angles). It can be appied to study atomic [21, 22] and molecular liquids [23, 24], glasses [25, 26], amorphous molecular systems [27] and crystals [28, 29].

Simulations were carried out with version 2.2 of programme rmc_pot++ [30]. Besides the old features (e.g. simultaneous fit of several diffraction and EXAFS datasets using various coordination and bond angle constraints) this version has important new capabilities (e.g. X-ray data intensity fit, EXAFS E_0 correction, use of tabulated atomic potentials) that will be discussed in a dedicated paper. Among the new features the EXAFS E_0 correction was used in the present study. This option allows to correct for the uncertainties of edge positions coming either from experimental calibration or from the determination of Fermi level. EXAFS backscattering factors were obtained by the feff8.4 programme [31]. The densities of the compositions investigated are given in Table 1.

We note here that due to poorer signal statistics the useful *k*-range of Ag K-edge data of $GeTe_4$-5Ag is shorter. Test simulation runs (using this truncated range for the Ag K-edge dataset of $GeTe_4$-15Ag) have shown that the shorter *k*-range does not affect the conclusions of this work.

The following simulation runs were carried out:

-test runs with 12000 atoms. The purpose of these runs was to check the necessity of Ge-Ag and Ag-Ag pairs. It was found that neither of these bonds is needed to fit the experimental data. Diffraction and EXAFS datasets of $(GeSe_3)_{0.435}$-$Ag_{0.565}$ (24.5 at.% Ag content) and GeS_3-25Ag could also be interpreted without Ge-Ag bonding [32, 33]. Ge-Ge and Ge-Ag cut offs were set to 3.2 Å and 3.3 Å while the Ge-Ge, Ge-Te, Te-Te and Te-Ag cut offs were equal to 3.5 Å, 2.3 Å, 2.4 Å and 2.5 Å, respectively. These runs also revealed that the first peak of $g_{GeTe}(r)$, the Ge-Te partial pair correlation function remains similar to that of $Ge_{19}Te_{81}$ [5] with increasing Ag content. Therefore it can be assumed that Ge remains fourfold coordinated by Te in $GeTe_4$-Ag glasses as well.

-'production runs' with 32000 atoms. The resulting configurations were used for detailed structural investigations. Initial configurations for these runs were obtained by placing atoms at random into a

cubic simulation box and moving them around to satisfy the above cut offs. In line with the observations of the test runs Ge atoms were constrained to have 4 Te neighbours. This constraint was satisfied by about 90-95% of Ge atoms. Neither the Te-Te coordination number nor the coordination number of Ag atoms was constrained.

-runs to estimate the uncertainty of coordination numbers of Te and Ag (the coordination number of Ge was supposed to be 4 therefore no uncertainty was calculated in this case). These runs were started from the configurations of the production runs. Average coordination constraints were used to perturb the coordination numbers in steps of ±5-10%. The R-factors were monitored and the resulting coordination numbers were considered to be incompatible with the data if the most relevant R-factor (e.g. that of the Ag K-edge EXAFS data in case of the Ag-Te coordination number) was increased by about 15% or spurious features (shoulder, sharp secondary maximum at the upper limit of the coordination sphere) appeared on the corresponding partial pair correlation functions.

Results and discussion

The $GeTe_4$ host network

Corrected experimental data are shown in Figures 1 and 2 while data of $GeTe_4$-15Ag and their fits are compared in Figures 3 and 4. Partial pair correlation functions are shown in Figures 5 and 6, together with the corresponding functions of binary $Ge_{19}Te_{81}$. Nearest neighbour distances and coordination numbers are given in Tables 2 and 3, respectively. The Ge-Te peak is at 2.61± 0.02 Å. This value agrees well with the mean Ge-Te distances found in Ge-Te [5], Ge-I-Te [8], Ge-Se-Te [10] and $Ag_5Ge_{15}Te_{80}$ glasses [34].

The Te-Te bond length increases gradually from 2.76 ± 0.02 Å to 2.81± 0.02 Å and the minimum around 3 Å becomes shallow upon adding Ag. In case of $GeTe_4$-15Ag even a pronounced shoulder can be observed. It is remarkable that the Te-Te coordination number (calculated up to 3.1 Å) still does not change significantly with the Ag content and the total number of Ge+Te atoms around Te remains very close to 2.

It was shown that the relatively sharp first peak of $g_{GeGe}(r)$ of $Ge_{19}Te_{81}$ is due to the dominance of corner sharing (CS) $GeTe_4$ tetrahedra [5]. Though the shape of the first peak of $g_{GeGe}(r)$ changes upon adding Ag (Fig. 5) a detailed analysis of the model configuration revealed that corner sharing is still the prevailing local configuration in $GeTe_4$-15Ag (Fig. 7).

The topology of the $GeTe_4$ network can also be described by N_{GeGe}, the Ge(-Ge) coordination number calculated up to the first minimum of $g_{GeGe}(r)$. It is to be emphasized that there are no Ge-Ge bonds in the model configurations therefore N_{GeGe} can rather be regarded as a measure of the connectivity of $GeTe_4$ tetrahedra. Rings of $GeTe_4$ tetrahedra are characterized by $N_{GeGe} = 2$ while for n-membered $GeTe_4$ tetrahedra chains, N_{GeGe} is equal to $2\text{-}2/n$ (if the contribution of topologically distant Ge atoms is negligible). It was found that for the glasses investigated, N_{GeGe} is equal to 1.83 ± 0.1 therefore the

average chain length is about 12. It should be kept in mind, however, that various combinations of chains and rings may give the same average N_{GeGe} and the distinction of these motifs is not possible by using diffraction or EXAFS data.

The number of Te atoms having two Ge neighbors (bridging Te atoms) can also be used to quantify network connectivity. Distributions of bridging Te atoms around Ge in $GeTe_4$-15Ag and $Ge_{19}Te_{81}$ are compared in Table 4. It can be concluded that though Ge-Ge, Ge-Te and Te-Te distance distributions are rearranged upon adding Ag, there are no significant differences in the connectivity of $GeTe_4$ tetrahedra in $Ge_{19}Te_{81}$ and $GeTe_4$-Ag glasses at the level of distribution of corner and edge sharing $GeTe_4$ tetrahedra and bridging Te atoms.

The environment of Ag atoms

Ag-related partial pair correlation functions are shown in Figure 6. The mean Ag-Te distance is around 2.76 ± 0.03 Å. This value agrees well with the Ag-Te bond lengths found in glassy $Ge_{15}Te_{80}Ag_5$ (2.77 Å ± 0.02 Å), $As_{34}Te_{51}Ag_{15}$ (2.78 Å ± 0.03 Å) and $GeTe_4$-AgI (2.80 ± 0.02 Å) [34, 35, 11]. We note here that due to the low Ag concentration, the uncertainty of Ag-Te distance was somewhat higher in case of $GeTe_4$-5Ag. The Ag(-Te) coordination numbers scatter around 2.6-2.7 not far from the result of Sakurai et al [34] who obtained 2.5 in $Ge_{15}Te_{80}Ag_5$. The average number of Te atoms around Ag in 0.75$GeTe_4$-0.25AgI was found to be 2.5 ± 0.4 [11]. In the latter composition, Ag-I bonds were also found and the total average coordination number of Ag atoms is 3.19 ± 0.3. As it has already been mentioned above, fits of experimental datasets do not improve if Ag-Ag bonds are allowed in the models generated by RMC. Thus, the Ag-Ag coordination number does not exceed the sensitivity of our aproach (~0.4) and the total average coordination number of Ag is not higher than 3. As the average Te-Ag coordination number does not change significantly with composition it can be assumed that the local environment of Ag is similar in all investigated glasses. A detailed investigation of the model configuration of GeTe4-15Ag revealed that Ge and Ag below 4.8 Å separation have mostly 0 (39%) or 1 (58%) common Te neighbour. This observation suggests that Ag avoids the edges or faces of $GeTe_4$ tetrahedra and is close to the short Te-chains connecting Ge atoms (as $N_{TeGe} \approx 1$ the dominance of corner sharing $GeTe_4$ tetrahedra entails the presence of Te-chains consisting of at least 3 Te atoms). Given its positive charge it can also be supposed that Ag is preferentially located at the non bonding electron pairs of Te atoms.

The conductivity of $GeTe_4$-Ag glasses was investigated by Cui et al [36]. It was found that the DC conductivity of $GeTe_4$-Ag glasses is mostly of electronic nature and increases monotonically with Ag content. These results are in line with the structural observations made in the present study: the concentration of charge carriers increases with increasing Ag content while the topology of the $GeTe_4$ host framework is largely preserved. The interplay of these two factors results in increased electronic conductivity.

Conclusions

The microscopic structure of $GeTe_4$-Ag glasses was modelled by fitting neutron diffraction, X-ray diffraction and EXAFS datasets simultaneously in the framework of the reverse Monte Carlo simulation technique. It has been revealed that at the level of coordination numbers the short-range order of the host $GeTe_4$ network remains unchanged upon adding Ag: Ge atoms are coordinated by four Te atoms and Te atoms have predominantly two Ge/Te neighbours. The distribution of bridging Te atoms around Ge also seems to be unaffected by the presence of Ag. Ag binds predominantly to Te and the total average coordination number of Ag does not exceed three.

Acknowledgments

P. J. is indebted to B. Klee and B. Paulus (University of Marburg) for helpful discussions. The neutron diffraction experiment was carried out at the Orphée reactor. P. J. was supported by the ELKH (Eötvös Loránd Research Network) grant 'Structure of energy storage materials'. High energy X-ray diffraction measurements were carried out with the support of Diamond Light Source, instrument I12-JEEP (nt21642-1). EXAFS measurements described in this paper were performed at the Canadian Light Source, a national research facility of the University of Saskatchewan, which is supported by the Canada Foundation for Innovation (CFI), the Natural Sciences and Engineering Research Council (NSERC), the National Research Council (NRC), the Canadian Institutes of Health Research (CIHR), the Government of Saskatchewan, and the University of Saskatchewan.

References

[1] B. Bureau, S. Danto, H.L. Ma, C. Boussard-Plédel, X.H. Zhang, J. Lucas, Tellurium based glasses: A ruthless glass to crystal competition, Solid State Sci. 10 (2008) 427–433. doi:10.1016/j.solidstatesciences.2007.12.017.

[2] A. A. Piarristeguy, E. Barthélémy, M. Krbal, J. Frayret, C. Vigreux, A. Pradel, Glass formation in the Ge_xTe_{100-x} binary system: Synthesis by twin roller quenching and co-thermal evaporation techniques, J. Non-Cryst. Solids 355, (2009) 2088-2091. https://doi.org/10.1016/j.jnoncrysol.2009.04.072.

[3] C. Conseil, J.-C. Bastien, C. Boussard-Plédel, X.-H. Zhang, P. Lucas, S. Dai, et al., Te-based chalcohalide glasses for far-infrared optical fiber, Opt. Mater. Express 2 (2012) 1470. doi:10.1364/OME.2.001470.

[4] Z. Yang, P. Lucas, Tellurium-based far-infrared transmitting glasses, J. Am. Ceram. Soc. 92 (2009) 2920–2923. doi:10.1111/j.1551-2916.2009.03323.x.

[5] P. Jóvári, A. Piarristeguy, A. Pradel, I. Pethes, I. Kaban, S. Michalik, et al., Local order in binary Ge-Te glasses – An experimental study, J. Alloys Compd. 771 (2019) 268–273. doi:10.1016/j.jallcom.2018.08.323.

[6] I. Voleská, J. Akola, P. Jóvári, J. Gutwirth, T. Wágner, T. Vasileiadis, et al., Structure, electronic, and vibrational properties of glassy $Ga_{11}Ge_{11}Te_{78}$: Experimentally constrained density functional study, Phys. Rev. B 86 (2012) 094108. doi:10.1103/PhysRevB.86.094108.

[7] I. Pethes, A. Piarristeguy, A. Pradel, S. Michalik, R. Nemausat, J. Darpentigny, P. Jóvári, Short range order and topology of $Ge_xGa_xTe_{100-2x}$ glasses, J. Alloys Compd. 834 (2020) 155097. doi:10.1016/j.jallcom.2020.155097.

[8] P. Jóvári, I. Kaban, B. Bureau, A. Wilhelm, P. Lucas, B. Beuneu, et al., Structure of Te-rich Te-Ge-X (X = I, Se, Ga) glasses, J. Phys.: Condens. Matter 22 (2010) 404207. doi:10.1088/0953-8984/22/40/404207.

[9] A. Bouzid, T-L. Pham, Z. Chaker, M. Boero, C. Massobrio, Y-H. Shin, G. Ori, Quantitative assessment of the structure of $Ge_{20}Te_{73}I_7$ chalcohalide glass by first-principles molecular dynamics, Phys. Rev. B 103 (2020) 094204 doi: 10.1103/PhysRevB.103.094204 .

[10] L. Rátkai, C. Conseil, V. Nazabal, B. Bureau, I. Kaban, J. Bednarcik, et al., Microscopic origin of demixing in $Ge_{20}Se_xTe_{80-x}$ alloys, J. Alloys Compd. 509 (2011) 5190–5194. doi:10.1016/j.jallcom.2011.02.032.

[11] P. Jóvári, S. Cui, V. Nazabal, I. Kaban, B. Beuneu, M. Dussauze, et al., Network Rearrangement in AgI-Doped $GeTe_4$ Glasses, J. Am. Ceram. Soc. 98 (2015) 1034–1039. doi:10.1111/jace.13369.

[12] R.L. McGreevy, L. Pusztai, Reverse Monte Carlo simulation: A new technique for the determination of disordered structures, Mol. Simul. 1 (1988) 359–367. doi:10.1080/08927028808080958.

[13] M. Winterer, Reverse Monte Carlo analysis of extended X-ray absorption fine structure spectra of monoclinic and amorphous zirconia, J. Appl. Physics 88 (2000) 5635 doi: 10.1063/1.1319167

[14] G.J. Cuello, J. Darpentigny, L. Hennet, L. Cormier, J. Dupont, B. Homatter, B. Beuneu, 7C2, the new neutron diffractometer for liquids and disordered materials at LLB, J. Phys.: Conf. Ser. 746 (2016) 012020 doi.org/10.1088/1742-6596/746/1/012020.

[15] V.F. Sears, Neutron scattering lengths and cross sections, Neutron News 3 (1992), 26-37 doi: 10.1080/10448639208218770

[16] H.H. Paalman, C.J. Pings, Numerical evaluation of x-ray absorption factors for cylindrical samples and annular sample cells, J. Appl. Phys. 33, 2635 – 2639 (1962) doi: 10.1063/1.1729034

[17] J. Filik, A.W. Ashton, P.C.Y. Chang, P.A. Chater, S.J. Day, M. Drakopoulos, et al., Processing two-dimensional X-ray diffraction and small-angle scattering data in DAWN 2, J. Appl. Crystallogr. 50 (2017) 959–966. doi:10.1107/S1600576717004708.

[18] X. Qiu, J.W. Thompson, S.J.L. Billinge, PDFgetX2 : a GUI-driven program to obtain the pair distribution function from X-ray powder diffraction data, J. Appl. Crystallogr. 37 (2004) 678–678. doi:10.1107/S0021889804011744.

[19] T. E. Faber & J. M. Ziman, Philosophical Magazine, A theory of the electrical properties of liquid metals 11 (1965) 153-173. doi: 10.1080/14786436508211931.

[20] K. V. Klementev, Extraction of the fine structure from x-ray absorption spectra, J. Phys. D: Appl. Phys. 34 (2001) 209–217. doi:10.1088/0022-3727/34/2/309.

[21] M. A. Howe, R. L. McGreevy, L. Pusztai, I. Borzsák, Determination of 3 body correlations in simple liquids by RMC modelling of diffraction data. 2. Elemental liquids, Phys. Chem. Liq. 25 (1993), 205-241. doi:10.1080/00319109308030363

[22] Q. Wang, C. Li, X. Niu, R. Shen, K. Lu, S. Wei, Z. Wu, T. Liu, Y. Xie, T. Hu, Structure of liquid krypton under atmospheric pressure: An EXAFS and reverse Monte Carlo study Phys. Rev. B 72 (1993) 092202 doi: 10.1103/PhysRevB.72.092202

[23] Sz. Pothoczki, L. Pusztai, Molecular liquid $TiCl_4$ and VCl_4: Two substances, one structure?, J. Mol. Liq. 145 (2009) 38-40. doi: 10.1016/j.molliq.2008.11.012

[24] I. Pethes; L. Pusztai, Reverse Monte Carlo investigations concerning recent isotopic substitution neutron diffraction data on liquid water, J. Mol. Liq. 212 (2015) 111-116. doi: 10.1016/j.molliq.2015.08.050

[25] P. Kidkhunthod, L. B. Skinner, A. C. Barnes, W. Klysubun, H. E. Fischer, Structure of Ba-Ti-Al-O glasses produced by aerodynamic levitation and laser heating, Phys. Rev. B 90 (2014) 094206. doi: 10.1103/PhysRevB.90.094206

[26] C. Gejke, J. Swenson, R. G. Delaplane, L. Börjesson, Neutron diffraction study of microscopic structure of SnB_2O_4 glass Phys. Rev. B 65 (2002) 212201. doi: 10.1103/PhysRevB.65.212201

[27] B. D. Klee, E. Dornsiepen, J. R. Stellhorn, B. Paulus, S. Hosokawa, S. Dehnen, W-C Pilgrim, Structure Determination of a New Molecular White-Light Source, Phys. Status Solidi B (2018) 1800083 https://DOI: 10.1002/pssb.201800083

[28] J. Du, A. E. Phillips, D. C. Arnold, D. A. Keen, M. G. Tucker, M. T. Dove Structural study of bismuth ferrite $BiFeO_3$ by neutron total scattering and the reverse Monte Carlo method, Phys. Rev. B 100 (2019) 104111. doi: 10.1103/PhysRevB.100.104111

[29] V. Dyadkin, F. Mushenok, A. Bosak, D. Menzel, S. Grigoriev, P. Pattison, D. Chernyshov, Structural disorder versus chiral magnetism in $Cr_{1/3}NbS_2$, Phys. Rev. B 91 (2015) 184205. doi: 10.1103/PhysRevB.91.184205

[30] O. Gereben, P. Jóvári, L. Temleitner, L. Pusztai, A new version of the RMC++ Reverse Monte Carlo programme, aimed at investigating the structure of covalent glasses, J. Optoelectron. Adv. Mater. 9 (2007) 3021–3027.

[31] A. L. Ankudinov, B. Ravel, J.J. Rehr, S.D. Conradson, Real-space multiple-scattering calculation and interpretation of x-ray-absorption near-edge structure, Phys. Rev. B 58 (1998) 7565–7576. doi:10.1103/PhysRevB.58.7565.

[32] L.S.R. Kumara1, K. Ohara, Y. Kawakita, P. Jóvári, M. Hidaka, N. E. Sung, B. Beuneu, S. Takeda, Local Structure of Superionic Glass $Ag_x(GeSe_3)_{1-x}$, x=0.565, EPJ Web of Conferences 15, 02007 (2011) doi: 10.1051/epjconf/20111502007

[33] L. Rátkai, I. Kaban, T. Wágner, J. Kolář, S. Valková, I. Voleská, B. Beuneu, P. Jóvári, Silver environment and covalent network rearrangement in GeS_3–Ag glasses, J. Phys.: Condens. Matter 22 (2010) 404207, doi: 10.1088/0953-8984/25/45/454210

[34] M. Sakurai, F. Kakinuma, E. Matsubara, K. Suzuki, Partial structure analysis of amorphous $Ge_{15}Te_{80}M_5$ (M=Cu, Ag and In), J. Non-Crystal. Solids 312–314 (2002) 585-588. doi:10.1016/S0022-3093(02)01789-1

[35] I. Kaban, W. Hoyer, P. Jóvári, T. Petkova, A. Stoilova, A. Schöps, J. Bednarcik, B. Beuneu, Atomic Structure of $As_{34}Se_{51}Ag_{15}$ and $As_{34}Te_{51}Ag_{15}$ Glasses Studied with Xrd, Nd and Exafs and Modeled withRMC, In: Reithmaier J.P., Petkov P., Kulisch W., Popov C. (eds) Nanostructured Materials for Advanced Technological Applications. NATO Science for Peace and Security Series B: Physics and Biophysics. Springer, Dordrecht. doi: 10.1007/978-1-4020-9916-8_37

[36] S. Cui, D. Le Coq, C. Boussard-Plédel, B. Bureau, Electrical and optical investigations in Te–Ge–Ag and Te–Ge–AgI chalcogenide glasses, J. Alloys Compd. 639 (2015) 173–179. doi: 10.1016/j.jallcom.2015.03.138

Table 1 Densities and glass transition temperatures of the $GeTe_4$-Ag glasses investigated

Sample name	$GeTe_4$	$GeTe_4$-5Ag	$GeTe_4$-10Ag	$GeTe_4$-15Ag
Composition	$Ge_{19}Te_{81}$	$Ge_{19}Te_{75}Ag_6$	$Ge_{18}Te_{72}Ag_{10}$	$Ge_{18}Te_{67}Ag_{15}$
Density (g/cm^3)	5.52	5.734	5.858	6.023
T_g (°C)	157	146	148	148

Table 2. Ge-Te, Te-Te and Te-Ag nearest neighbor distances in $GeTe_4$-Ag, $Ge_{19}Te_{81}$, $0.75GeTe_4$-0.25AgI and $Ge_{20}I_7Te_{73}$ glasses. Values are given in Å. The uncertainty of Ge-Te and Te-Te nearest neighbour distances is around ± 0.02 Å

	r_{GeTe} [Å]	r_{TeTe} [Å]	r_{TeAg} [Å]
$Ge_{19}Te_{81}$ [5]	2.61	2.76	-
$GeTe_4$-5Ag	2.60	2.75	2.73 ± 0.04
$GeTe_4$-10Ag	2.62	2.76	2.75 ± 0.03
$GeTe_4$-15Ag	2.60	2.79	2.78 ± 0.03
$0.75GeTe_4$-0.25AgI [9]	2.62	2.78	2.80 ± 0.02
$Ge_{20}I_7Te_{73}$ [7]	2.61	2.72	-

Table 3. Coordination numbers in $GeTe_4$-Ag glasses obtained by reverse Monte Carlo simulation. Corresponding values of $Ge_{19}Te_{81}$, $0.75GeTe_4$-0.25AgI and $Ge_{20}I_7Te_{73}$ are also shown for comparison.

	N_{GeTe}	N_{TeGe}	N_{TeTe}	N_{TeAg}	N_{AgTe}	N_{Ge}	N_{Te}	N_{Ag}
$Ge_{19}Te_{81}$	4.1(-0.2 + 0.6)	0.9(-0.05 +0.15)	1.06±0.15	-	-	4.10	2.0±0.1	-
$GeTe_4$-5Ag	3.90	0.99	0.9±0.2	0.26±0.7	3.2±0.8	3.90	2.1±0.1	3.2±0.8
$GeTe_4$-10Ag	4.05	1.01	1.0±0.2	0.36±0.07	2.6±0.5	4.05	2.3±0.1	2.6±0.5
$GeTe_4$-15Ag	4.02	1.08	1.0±0.2	0.56±0.1	2.5±0.5	4.02	2.7±0.2	2.5±0.5
$0.75GeTe_4$-0.25AgI	3.77	0.94	1.82±0.3	0.21±0.03	2.5±0.4	3.94	2.97±0.3	3.19±0.5
$Ge_{20}Te_{73}$ I_7	3.73	1.02	1.00	-	-	4.02	2.0±0.1	-

Table 4. Distribution of the number of bridging Te atoms (having two Ge nearest neighbors) around Ge in glassy $Ge_{19}Te_{81}$ and $GeTe_4$-15Ag

	0	1	2	3	4
$Ge_{19}Te_{81}$	7.9%	28.0%	36.5%	22.6%	5.1%
$GeTe_4$-15Ag	7.5%	31.2%	38.5%	19.6%	3.2%

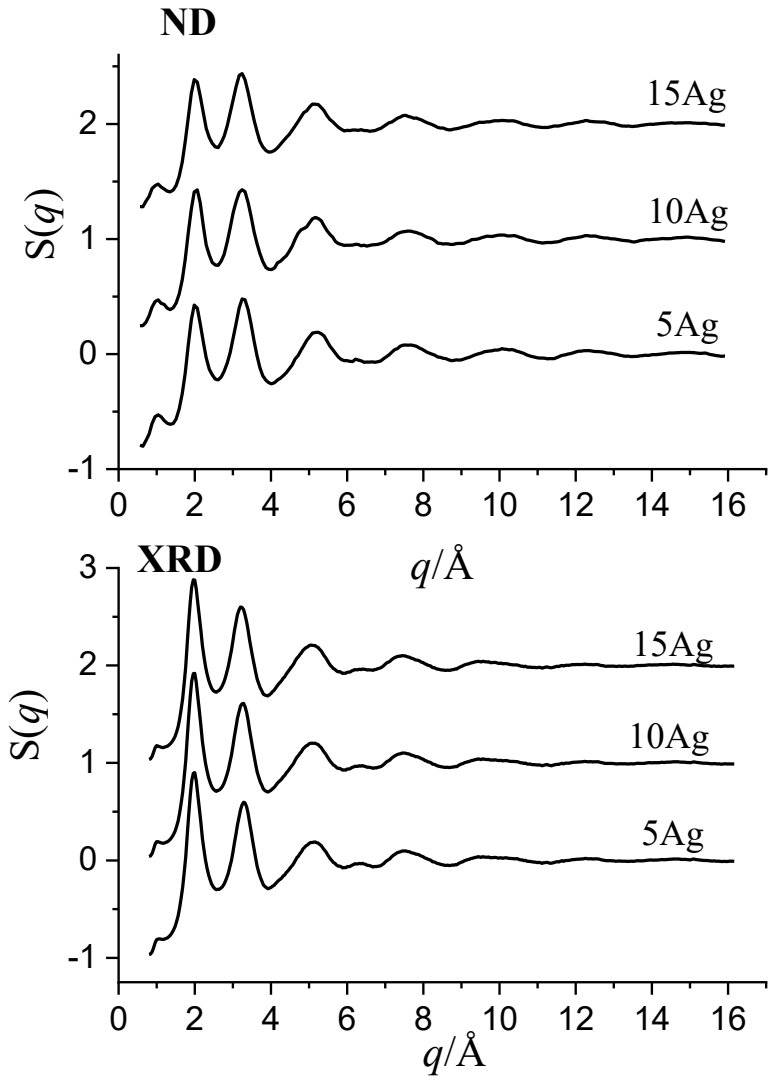

Figure 1. Neutron (upper panel) and X-ray diffraction structure factors of the investigated $GeTe_4$-Ag glasses. Curves of $GeTe_4$-10Ag and $GeTe_4$-15Ag are shifted vertically with 1 and 2 units, respectively.

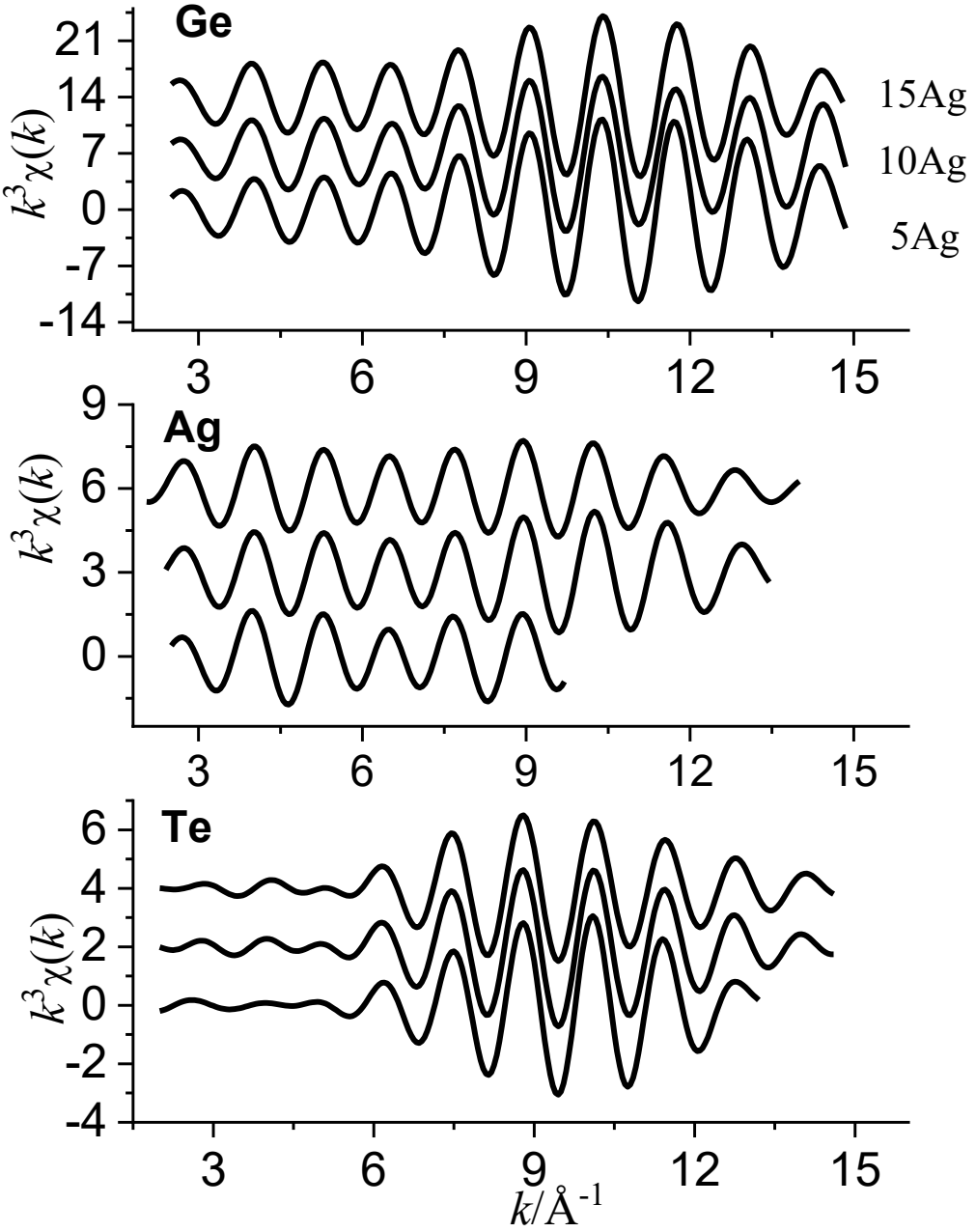

Figure 2. k^3-weighted and filtered Ge-, Ag- and Te K-edge EXAFS $\chi(k)$ functions of the investigated $GeTe_4$-Ag glasses. Curves of $GeTe_4$-10Ag and $GeTe_4$-15Ag are shifted vertically for clarity.

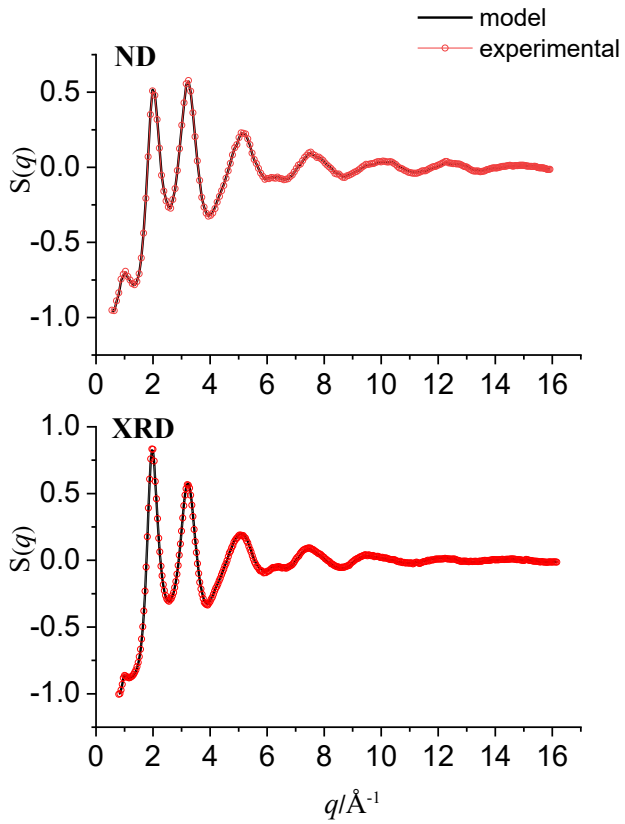

Figure 3. Comparison of experimental neutron- and X-ray diffraction structure factors with the corresponding model curves obtained by fitting simultaneously the five experimental datasets of $GeTe_4$-15Ag.

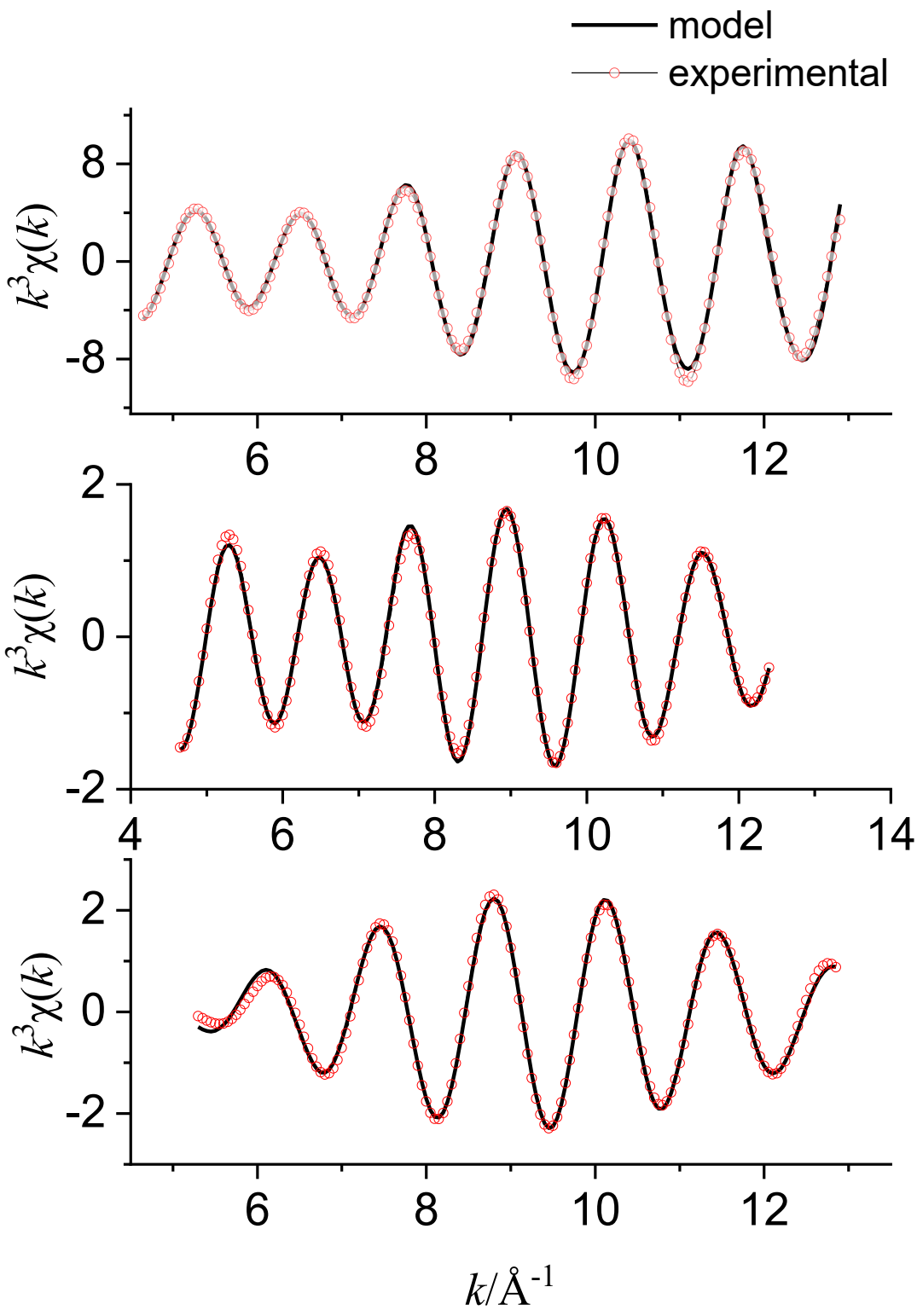

Figure 4. Comparison of experimental Ge, Ag- and Te K-edge $k^3\chi(k)$ functions with the corresponding model curves obtained by fitting simultaneously the five experimental datasets of $GeTe_4$-15Ag.

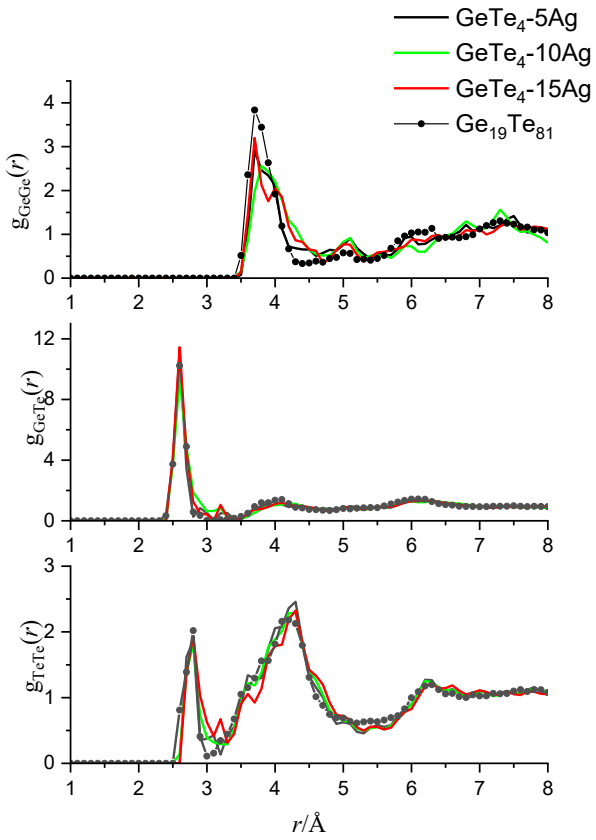

Figure 5. Ge-Ge, Ge-Te and Te-Te pair correlation functions of $Ge_{19}Te_{81}$ and the investigated $GeTe_4$-Ag glasses.

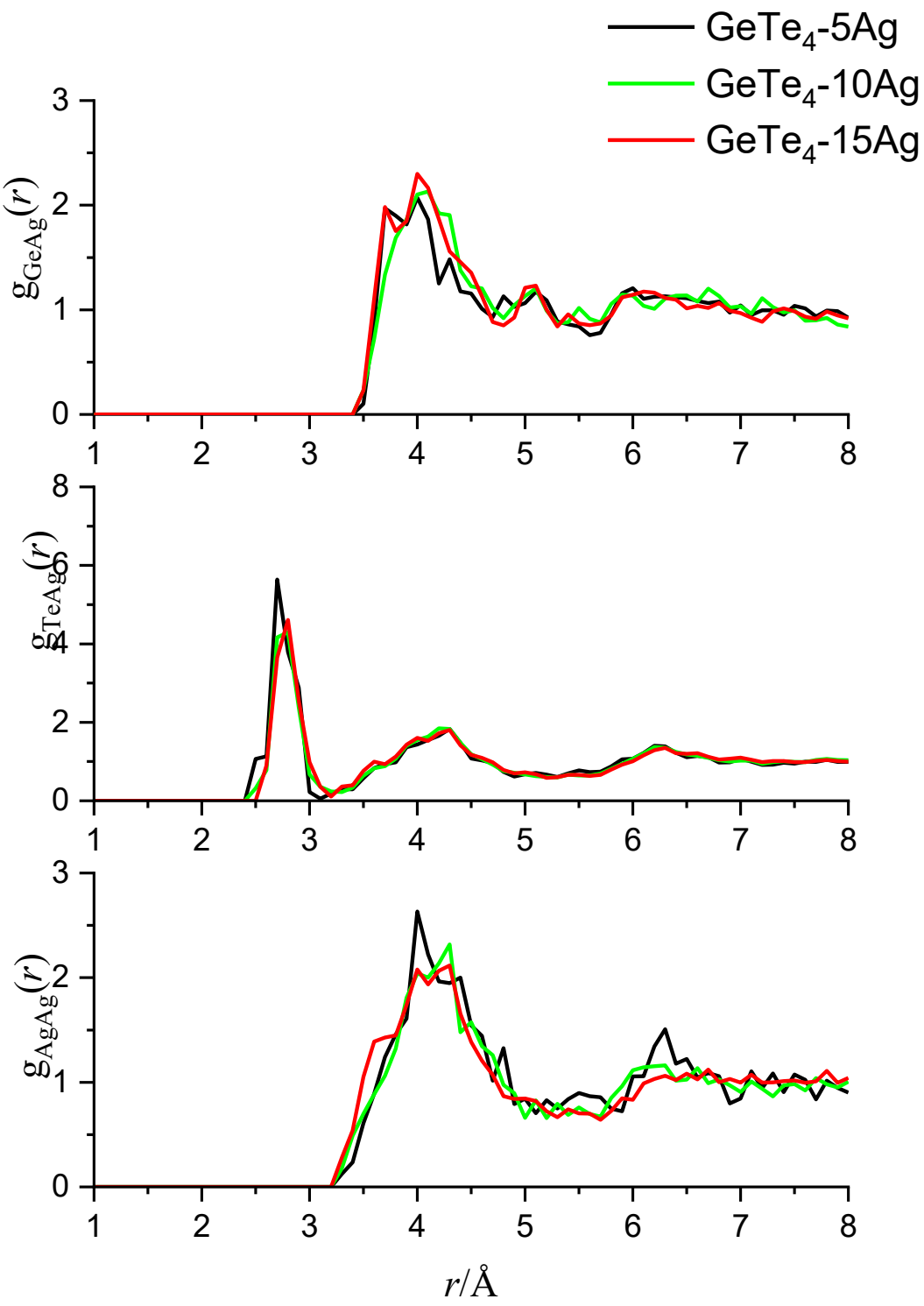

Figure 6. The Ge-Ag, Te-Ag and Ag-Ag partial pair correlation functions of $GeTe_4$-Ag glasses

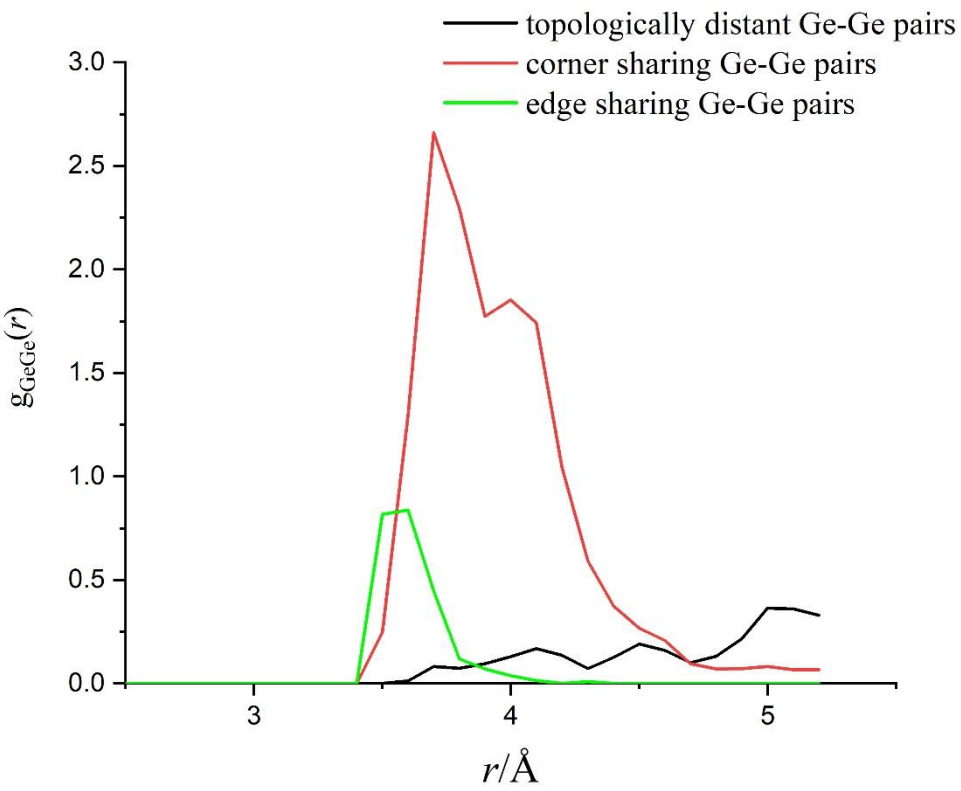

Figure 7. Decomposition of the first peak of $g_{GeGe}(r)$ of $GeTe_4$-15Ag into contributions from Ge-Ge pairs centering edge and corner sharing $GeTe_4$ tetrahedra and topologically distant Ge-Ge pairs.